2026 IEEE International Conference on Robotics and Automation (ICRA 2026)
June 1-5, 2026. Vienna, Austria

A Novel Tilting Mechanism for Personal Mobility Robot Platform: Mathematical Modeling and HILS-Based Control Verification

Sunyeop Lee[1†], Wonchang Yang[2†], Yongseob Lim[2*], and Kanghyun Nam[2*]

Abstract— **This paper introduces a suspension-integrated tilting mechanism for narrow-track mobility robot platforms, offering a novel means of achieving commanded body tilt without departing from conventional suspension layouts. The architecture provides a two-degree-of-freedom roll path with inherent passive self-centering, thereby reconciling mechanical simplicity with enhanced motion capability. A linearized dynamic model forms the foundation for a dual-layer control scheme, consisting of a reference generator and a high-bandwidth tracking loop. The proposed approach is rigorously evaluated through hardware-in-the-loop simulations that combine a real-time driving simulator with a physical hardware bench. Relative to a non-tilting baseline, the platform demonstrates substantial reductions in perceived lateral acceleration and lateral load transfer, signifying improved ride comfort and rollover stability. These findings establish suspension-integrated tilting with model-based control as a compelling pathway toward safe and stable next-generation mobility robot platforms.**

I. INTRODUCTION

Growing urban populations, emission regulations, and parking shortages are shifting demand toward compact personal mobility [1]. These platforms occupy less road space but are required to provide maneuverability and comfort similar to larger classes. A direct consequence of the narrow track is a lower rollover threshold, which can be seen from the Static Stability Factor $\mathrm{SSF} = T_w/(2h_{\mathrm{cg}})$: when the track T_w is small relative to the center-of-mass height h_{cg}, the lateral acceleration required for wheel lift is reduced [2]. As a result, securing rollover safety for narrow-track compact mobility is essential.

Tilting mobility addresses this problem by leaning the cabin toward the inside of a turn so that the apparent gravity aligns with the cabin vertical and the driver feels less lateral load. Hardware implementations of tilting mobility can be mainly classified into two families: chassis tilting [3], [4], [5] and cabin tilting [6]. In chassis tilting, the body and wheel assemblies tilt together about a tilting axis. In cabin tilting, the cabin leans while the suspensions remain nearly upright. Each choice carries trade-offs in mechanism complexity, suspension impact, and driver comfort. In addition, architectures such as cabin tilting and chassis tilting can be formulated on a bicycle-model basis to derive the tilting dynamics [7], [8], [9]; they are typically represented by a single inverted pendulum, that is, a one-degree-of-freedom (1-DOF) tilting model.

In this study, we adopt a third option called a suspension-integrated layout [10], [11], where the upper mount of a MacPherson strut is connected to a tilting plate and the plate is actuated relative to the cabin. This keeps a familiar suspension topology, enables commanded tilting, and provides passive self-centering from gravity and spring forces at standstill. Prior studies often assume an actuator that applies torque directly to the body about a fixed hinge [19]. In contrast, the suspension-integrated mechanism couples the cabin and the plate, creating a two-degree-of-freedom (2-DOF) tilting path through both the body and the suspensions. To control rollover safety of this 2-DOF architecture, a clear mathematical description is necessary. Therefore, we derive an analytical model for the mechanism and obtain a linear state-space form around small tilting angles for controller design. To quantitatively assess the safety of the control, objective metrics are required. Two complementary indicators are the driver-perceived lateral acceleration and the lateral load transfer ratio (LTR) [12], [13], [14], which measures the normalized left and right vertical load shift. For tilting mobility with cabin-tilting or chassis-tilting layouts, various control strategies have been explored, including schemes that command body torque directly [15], [16], [17] and schemes that regulate the tilting angle explicitly [18], [19], [20], [21]; among them are approaches that address nonlinear effects [22]. For the 2-DOF tilting structure proposed in this work, an angle-tracking strategy grounded in the derived model is more suitable than generating a direct torque command. These considerations suggest a dual-layer control structure: an tilt-reference generator that generates a target tilting angle ϕ_t^* to reduce perceived lateral acceleration in cornering, and an tilt-tracking controller that tracks ϕ_t with high bandwidth and robustness.

Hardware-in-the-loop simulation (HILS) can effectively verify tilting control because it allows realistic interaction between computational mobility dynamics and physical actuation, including actuator limits, gearbox friction, and sensor noise. In this work, the HILS environment couples a real-time driving simulator with an embedded control computer and a hardware bench that reproduces roll moments seen in driving, enabling repeatable evaluation under constant-radius cornering, double lane change, and driver-in-the-loop manual driving.

†These authors contributed equally to this work (co-first authors).
*Corresponding authors: Yongseob Lim and Kanghyun Nam.

This work was supported by the Korea Evaluation Institute of Industrial Technology (KEIT) grant funded by the Korea government (MOTIE) (Nos. RS-2025-25454758 and RS-2024-00402701).

[1]Sunyeop Lee is with R1 Team, SUM Co., Ltd., FMTC 301, 82 Baegot 2-ro, Siheung-si, Gyeonggi-do, Republic of Korea (e-mail: yeop3114@smobi.ai).

[2]Wonchang Yang, Yongseob Lim, and Kanghyun Nam are with the Department of Robotics and Mechatronics Engineering, Daegu Gyeongbuk Institute of Science and Technology (DGIST), Daegu, Republic of Korea (e-mail: {wchyang, yslim73, khnam}@dgist.ac.kr).

II. NOVEL TILTING MECHANISM

Compact personal mobility has a narrow track, which lowers the rollover threshold. A simple static indicator is the Static Stability Factor (SSF),

$$\mathrm{SSF} = \frac{T_w}{2h_{cg}}, \tag{1}$$

where T_w is the track width and h_{cg} is the center-of-gravity height. A smaller SSF implies a lower lateral acceleration level for wheel lift, which motivates an active tilting mechanism.

Prior layouts are broadly classified into chassis tilting and cabin tilting. Figure 1 summarizes the two families and the present concept used in this work.

The proposed mechanism connects the upper mount of a MacPherson strut to a tilting plate instead of fixing it directly to the body. An actuator placed between the plate and the cabin rotates the plate relative to the cabin. The motor torque splits into two paths: the shaft side drives the plate and changes the suspension geometry, while the housing side reacts on the cabin as a roll moment. This is represented by

$$T_m = T_{\text{shaft}} - M_{\text{tilt}}, \qquad \phi_m = \phi_{\text{shaft}} - \phi_t, \tag{2}$$

where T_m is the commanded motor torque, T_{shaft} is the torque transmitted through the motor shaft to the plate, and M_{tilt} is the reaction (roll) torque applied to the cabin through the motor housing. Here ϕ_t denotes the cabin tilting (roll) angle, ϕ_m is the plate angle relative to the cabin, and ϕ_{shaft} is the plate absolute angle (identical to ψ in Sec. III); angles are defined positive for inside-leaning roll.

A practical benefit of this layout is self-centering at standstill and in steady cruising without extra centering springs. For small tilting angles, the left and right strut lengths vary as $l_{l,r} \approx L_0 \pm c\,\phi_t$, where l_l and l_r are the left/right strut lengths, L_0 is the natural (unloaded) strut length, and c is the effective geometric lever from cabin tilt to strut extension. The axial spring forces become $F_{l,r} \approx K(l_{l,r} - L_0)$, with K the strut axial stiffness. The resulting left–right force difference is $\Delta F \equiv F_l - F_r \approx 2Kc\,\phi_t$, and the induced roll moment is

$$M_{\text{spring}} \approx \frac{T_w}{2}\Delta F = K_\phi\,\phi_t, \qquad K_\phi \equiv K\,T_w\,c, \tag{3}$$

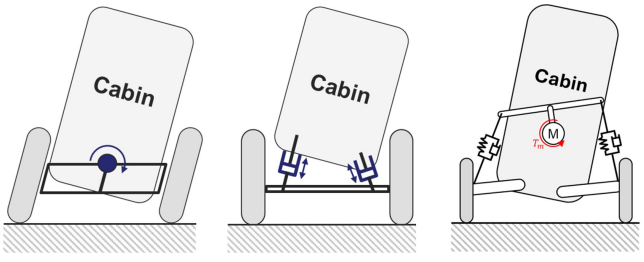

(a) (b) (c)

Fig. 1: Tilting layouts: (a) chassis tilting; (b) cabin tilting; (c) proposed suspension-integrated layout.

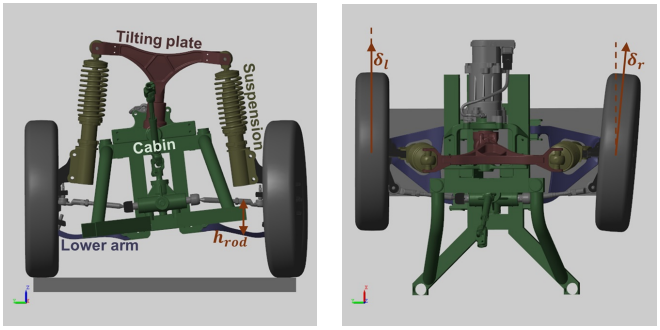

(a) (b)

Fig. 2: MacPherson-based suspension-integrated tilting mobility: (a) rear view; (b) upper view

where T_w is the track width and K_ϕ is the effective roll stiffness contributed by the suspensions. Together with gravity $M_g \approx mgh\,\phi_t$, the passive restoring moment is $(K_\phi + mgh)\phi_t$,where m is the equivalent sprung mass contributing to roll and h is the center-of-mass height above the roll center (m). Therefore, $\phi_t = 0$ is a stable equilibrium when $T_m = 0$.

TABLE I: Symbols

Symbol	Meaning (units)
ϕ_t	Cabin tilting angle (rad, absolute)
ϕ_m	Plate angle relative to cabin (rad)
ψ	Plate absolute angle (rad)
T_m	Commanded motor torque (N m)
h	Height of center of mass above roll center (m)
h_m	Height of motor shaft (m)
w	Half-length of plate bar (m)
w_{arm}	Lower suspension anchor x-offset (m)
m_c, m_p	Mass of cabin/plate (kg)
J_c	Cabin rotary inertia about roll center O (kg m^2)
J_p	Plate rotary inertia about hinge (kg m^2)
K, C	Axial spring/damper coefficients (N/m, N s/m)
B	Relative rotational damping (N m s/rad)
L_0	Natural spring length (m)
g	Gravity (m/s^2)
T_w	Track width (m)
h_{cg}	Height of vehicle center of gravity (m)
SSF	Static Stability Factor (-)
v_x	Longitudinal speed (m/s)
δ_f	Front-wheel steer angle (rad)
L	Wheelbase (m)
$F_{z,l}, F_{z,r}$	Left/right vertical wheel loads (N)
LTR	Load transfer ratio (-)

III. MATHEMATICAL MODELING

Figure 3 illustrates how the tilting mechanism is abstracted to the analytical model used in this paper: the cabin behaves as an inverted pendulum rotating about the roll center, a straight bar represents the tilting plate, and each suspension is a massless axial spring-damper from a fixed lower anchor to the plate upper joint. Knuckles rotate about fixed axes without lateral translation, lower arm forces and suspension-induced vertical motions (bump/bound) are neglected, and tire stiffness is ignored to focus on tilting dynamics.

Assumptions

- The cabin is an inverted pendulum about the roll center and is connected to ground by a revolute joint.
- The tilting plate is a single straight bar; knuckles rotate about fixed axes with no lateral displacement.
- Forces from lower arms are omitted; suspension bump/bound vertical motion is ignored.
- Tire forces are neglected because, in the operating range of interest, motions and loads induced by tilting dominate the local tire deflection effects.

A. Kinematics

Let the hinge position and the plate rotation be

$$r_0(\phi_t) = \begin{bmatrix} -h_m \sin\phi_t \\ h_m \cos\phi_t \end{bmatrix}, \quad R(\psi) = \begin{bmatrix} \cos\psi & -\sin\psi \\ \sin\psi & \cos\psi \end{bmatrix}. \tag{4}$$

With local plate points $p_R = [w\ 0]^\top$ and $p_L = [-w\ 0]^\top$, the upper joints are $r_{R/L} = r_0 + R(\psi)p_{R/L}$, and the fixed lower anchors are $a_R = [w_{\text{arm}}\ 0]^\top$, $a_L = [-w_{\text{arm}}\ 0]^\top$. Right/left suspension vectors and lengths are

$$d_R = r_R - a_R, \quad d_L = r_L - a_L, \quad l_r = \|d_R\|,\ l_l = \|d_L\|. \tag{5}$$

Linearizing about $(\phi_t, \phi_m) = (0,0)$ yields

$$L_{\text{base}} = \sqrt{(w - w_{\text{arm}})^2 + h_m^2}, \quad \alpha = \frac{h_m w_{\text{arm}}}{L_{\text{base}}},\ \beta = \frac{h_m w}{L_{\text{base}}}, \tag{6}$$

and the first-order lengths

$$l_r \approx L_{\text{base}} + \alpha\,\phi_t + \beta\,\phi_m, \tag{7}$$

$$l_l \approx L_{\text{base}} - \alpha\,\phi_t - \beta\,\phi_m. \tag{8}$$

For validation of the small-angle approximation, we define the absolute and normalized errors between the exact kinematics (5) and the linearized form (7) as

$$e_{r,l} \triangleq l_{r,l}^{\text{exact}} - l_{r,l}^{\text{lin}}, \qquad \varepsilon_{r,l} \triangleq \frac{e_{r,l}}{L_{\text{base}}}. \tag{9}$$

Figure 4 compares $l_{r,l}^{\text{exact}}$ and $l_{r,l}^{\text{lin}}$ for typical operating ranges ($\phi_t, \phi_m \in [-10^\circ, 10^\circ]$) and shows the approximation error. When both angles lie within $\pm 10^\circ$, the worst-case discrepancy is about 1.8°, occurring when ϕ_t and ϕ_m twist in opposite directions; under practical tilting trajectories, the maximum error remains near 1°.

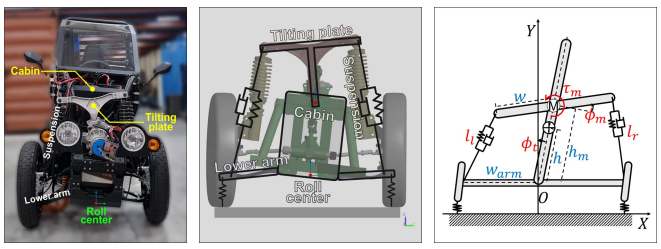

(a) (b) (c)

Fig. 3: Tilting mobility: (a) real-world prototype; (b) multibody model; (b) simplified model

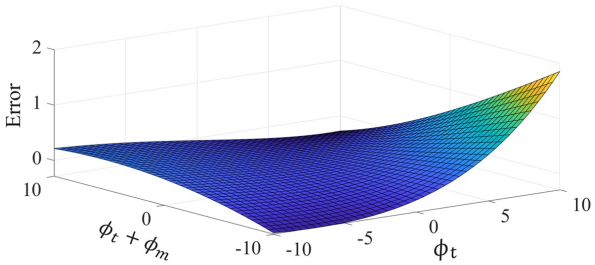

Fig. 4: Error of the linearized suspension length.

B. Dynamic equation

With the plate center of mass at the hinge, the kinetic energy is

$$T = \tfrac{1}{2}\left[\left(J_c + m_p h_m^2 + J_p\right)\dot{\phi}_t^2 + 2J_p\,\dot{\phi}_t\dot{\phi}_m + J_p\,\dot{\phi}_m^2\right]. \tag{10}$$

Potential and dissipation energies are

$$V_g = (m_c g h + m_p g h_m)\cos\phi_t, \tag{11}$$

$$V_s = \tfrac{1}{2}K\left[(l_r - L_0)^2 + (l_l - L_0)^2\right], \tag{12}$$

$$\mathscr{R} = \tfrac{1}{2}C\left(\dot{l}_r^2 + \dot{l}_l^2\right) + \tfrac{1}{2}B\,\dot{\phi}_m^2. \tag{13}$$

Let $q = [\phi_t\ \ \phi_m]^\top$ and $\tau = [0\ \ T_m]^\top$. The Lagrange equations with dissipation give

$$\frac{d}{dt}\left(\frac{\partial T}{\partial \dot{q}}\right) - \frac{\partial T}{\partial q} + \frac{\partial \mathscr{R}}{\partial \dot{q}} + \frac{\partial (V_g + V_s)}{\partial q} = \tau. \tag{14}$$

Let gravitational forces $k_g = -m_c g h - m_p g h_m$. Linearizing near zero tilting angle yields the mass, damping, and stiffness matrices

$$M = \begin{bmatrix} J_c + m_p h_m^2 + J_p & J_p \\ J_p & J_p \end{bmatrix}, \tag{15}$$

$$D = 2C\begin{bmatrix} \alpha^2 & \alpha\beta \\ \alpha\beta & \beta^2 \end{bmatrix} + \begin{bmatrix} 0 & 0 \\ 0 & B \end{bmatrix}, \tag{16}$$

$$K_{\text{t}} = 2K\begin{bmatrix} \alpha^2 + k_g & \alpha\beta \\ \alpha\beta & \beta^2 \end{bmatrix}. \tag{17}$$

Thus,

$$M\ddot{q} + D\dot{q} + K_{\text{t}} q = \tau. \tag{18}$$

With the state $x = [\phi_t\ \ \phi_m\ \ \dot{\phi}_t\ \ \dot{\phi}_m]^\top$ and input $u = T_m$,

$$\dot{x} = \begin{bmatrix} 0_{2\times 2} & I_2 \\ -M^{-1}K_{\text{t}} & -M^{-1}D \end{bmatrix} x + \begin{bmatrix} 0_{2\times 1} \\ M^{-1}e_2 \end{bmatrix} u, \tag{19}$$

when let $e_2 = [0\ 1]^\top$.

The linear state-space model (19) was then compared with a nonlinear multibody reference; Figure 5 shows close agreement for velocities of the model, supporting the use of the linear model for controller design and stability analysis.

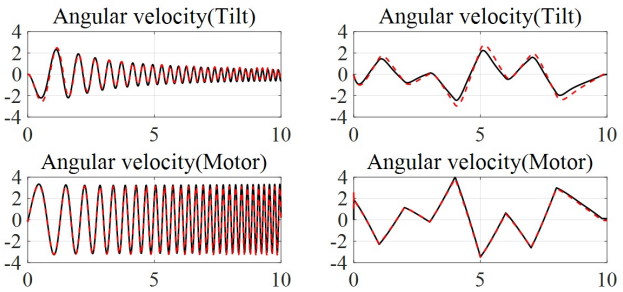

(a) (b)

Fig. 5: Validation of the linear state-space model: (a) chirp; (b) random

C. Transfer function

From $M\ddot{q}+D\dot{q}+Kq=\tau$, define the quadratics

$$A(s)=(J_c+m_p h_m^2+J_p)s^2+2C\alpha^2 s+(k_g+2K\alpha^2), \quad (20)$$

$$B(s)=J_p s^2+2C\alpha\beta\, s+2K\alpha\beta, \quad (21)$$

$$D(s)=J_p s^2+(2C\beta^2+B)s+2K\beta^2. \quad (22)$$

The tilting torque equation is

$$P(s)\triangleq\frac{\phi_t(s)}{T_m(s)}=\frac{B(s)}{B(s)^2-A(s)D(s)}, \quad (23)$$

which is a strictly proper $\frac{2\text{nd}}{4\text{th}}$ transfer function. For synthesis we use a reduced nominal plant $P_n(s)$ by fixing the operating point parameters.

TABLE II: Model and control parameters

Symbol	Value (units)	Symbol	Value (units)
m_c	550 (kg)	J_n	1.994e-6 (deg/A)
m_p	7 (kg)	B_n	5.012e-6 (deg/A)
h	0.43 (m)	ω_{fb}	8 (Hz)
h_m	0.31 (m)	ω_{ff}	50 (Hz)
K	9810 (N/m)	ω_Q	3 (Hz)
C	2400 (N s/m)	τ_{fb}	3.183e-3 (s)
B	120 (N m s/deg)	τ	0.106 (s)
		ζ	0.707 (-)
		k	0.3 (-)

IV. TILTING CONTROL AND HILS-BASED VALIDATION

A. Control structure and tilt-reference generator

The controller follows a dual-layer structure: (i) an tilt-tracking controller that tracks the tilting angle ϕ_t with high bandwidth and robustness, and (ii) an tilt-reference generator that generates a target tilting angle ϕ_t^* from the mobility state $(v_x,\ \delta_f)$ so as to reduce the perceived lateral acceleration in cornering.

Assuming quasi steady cornering and neglecting side-slip acceleration and tilting angular acceleration, the target angle that aligns apparent gravity with the cabin vertical is

$$\phi_t^*\approx\tan^{-1}\left(\frac{a_y}{g}\right)=\tan^{-1}\left(\frac{v_x^2}{gR}\right)\approx\frac{v_x^2}{gL}\,\delta_f. \quad (24)$$

For implementation it is convenient to separate the quasi-static mapping and the shaping dynamics:

$$C_{\text{Tilt}}\triangleq\frac{v_x^2}{gL},\qquad \phi_t^*(s)=C_{\text{Tilt}}\,G_{\text{Tune}}(s)\,\delta_f(s). \quad (25)$$

Here C_{Tilt} is updated online from measured v_x (and known L). The term $G_{\text{Tune}}(s)$ shapes responsiveness and magnitude:

$$G_{\text{Tune}}(s)=\frac{k}{\tau s+1},\qquad |\phi_t^*|\le\phi_{\max},\quad |\dot{\phi}_t^*|\le\dot{\phi}_{\max}. \quad (26)$$

The gain k adjusts the steady tilting level and τ moderates the response speed so that steering transients do not excite uncomfortable cabin motion. In practice, k and τ may be scheduled with v_x to keep the perceived response uniform across speed. Saturation limits $(\phi_{\max},\dot{\phi}_{\max})$ and a rate limiter prevent excessive demands on the actuator and protect ride comfort.

The steering signal is first low-pass filtered to suppress high-frequency noise from handwheel sensor. A plausibility check rejects spikes from sensor dropouts. A supervisor monitors actuator temperature and current; if a thermal or electrical limit is reached, the system blends ϕ_t^* to zero with a slow ramp to avoid abrupt posture changes. These interlocks act only on the tilt-reference generator and do not alter the inner-loop stability guarantees.

B. Tilting angle controller design

The torque-to-tilting angle plant is approximated by a second-order nominal model:

$$P_n(s)=\frac{\phi_t(s)}{T_m(s)}=\frac{1}{J_n s^2+B_n s}, \quad (27)$$

where J_n is the nominal roll inertia of the mobility and B_n is nominal viscous damping that aggregates bushing friction and the reduction-gear effects. Frequency-response identification on the bench shows almost no pronounced resonance or anti-resonance, which is consistent with the small tilting-plate mass relative to the cabin and the dominance of the gear train. Figure 7 illustrates the measured plant and the fit.

The tilt-tracking controller employs feedback (FB), feedforward (FF), and a disturbance observer (DOB) based on $P_n(s)$; see Figure 8. Here, τ_{fb} denotes the first-order low-pass shaping parameter (time constant) in $C_{FB}(s)$, ω_{fb} sets the feedback gain, and ω_{ff} sets the second-order low-pass filter bandwidth of the feedforward. The damping ratio (ζ) and the cut-off frequency of the DOB(ω_Q) set the band of the DOB.

$$C_{FB}(s)=\left(\frac{J_n s}{\tau_{fb}s+1}+B_n\right)\omega_{fb}, \quad (28)$$

$$C_{FF}(s)=\frac{(J_n s^2+B_n s)\,\omega_{ff}^2}{s^2+2\zeta\,\omega_{ff}s+\omega_{ff}^2}, \quad (29)$$

$$Q(s)=\frac{\omega_Q^2}{s^2+2\zeta\,\omega_Q s+\omega_Q^2}. \quad (30)$$

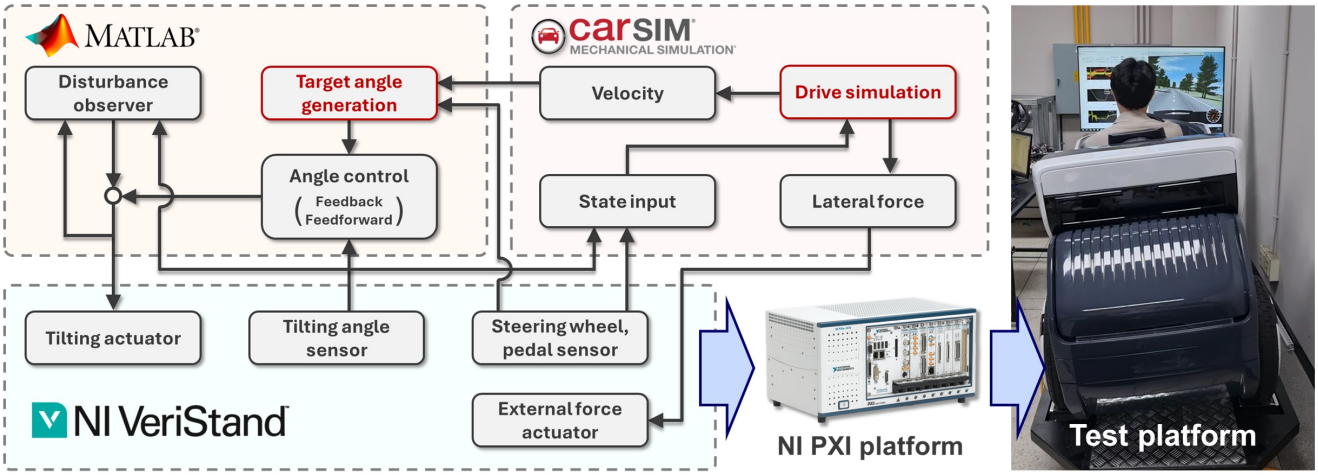

Fig. 6: Hardware and signal interface block diagram.

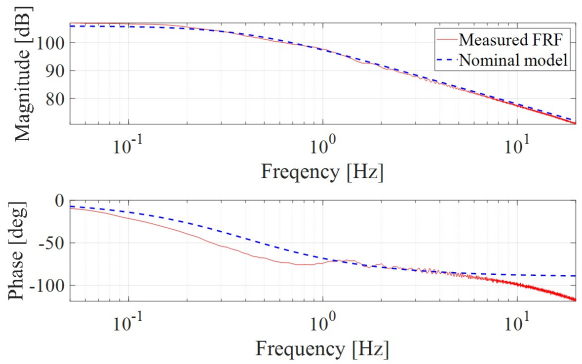

Fig. 7: Identification result of tilting model.

The feedback compensator cancels the nominal pole–zero pair to increase loop gain at low frequency without aggressive high-frequency amplification. The feedforward inverts $P_n(s)$ and is regularized by a second-order low-pass filter. The DOB estimates lumped disturbances (model mismatch, friction ripple, road-induced roll moments) by comparing the predicted nominal input to the actual input and filtering the difference through $Q(s)$ so that only the observable frequency band (set by ω_Q and ζ) is injected for compensation.

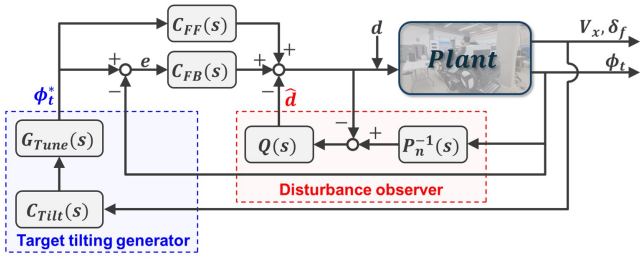

Fig. 8: Tilting angle control loop.

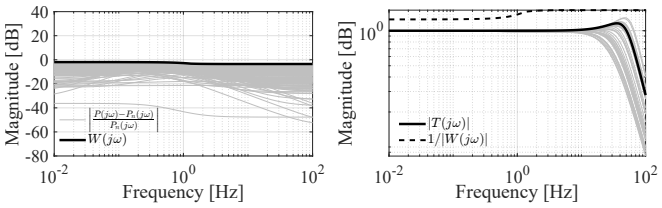

(a) (b)

Fig. 9: Frequency analysis for the uncertain model: (a) $|(P(j\omega)-P_n(j\omega))/P_n(j\omega)|$ and $|W(j\omega)|$; (b) $|T(j\omega)|$ and $|W(j\omega)|^{-1}$.

C. Robust Stability

To ensure stability against model mismatch and simplifications (Sec. III), the controller is tuned using the small-gain theorem. Parametric variations are represented by a family of plants $P(s) = 1/(Js^2+Bs)$, where $J \in [0.7,3]J_n$ and $B \in [0.7,5]B_n$. The mismatch is modeled as multiplicative uncertainty:

$$\left|\frac{P(j\omega)-P_n(j\omega)}{P_n(j\omega)}\right| \le |W(j\omega)|, \tag{31}$$

where $W(j\omega)$ envelopes the relative errors (Fig. 9(a)). Robust stability is guaranteed if the complementary sensitivity $T(s) = L(s)/(1+L(s))$ satisfies the small-gain condition:

$$|T(j\omega)| < |W(j\omega)|^{-1}, \quad \forall \omega. \tag{32}$$

As shown in Fig. 9(b), the condition is satisfied with a sufficient margin. This confirms that the nominal-model-based control remains robustly stable despite high-order dynamics and variations not captured in the simplified plant $P_n(s)$.

D. HILS configuration

The HILS platform couples (i) CarSim for driving scenarios and tire-road reactions, (ii) MATLAB/Simulink for real-time control computation, and (iii) a VeriStand-based

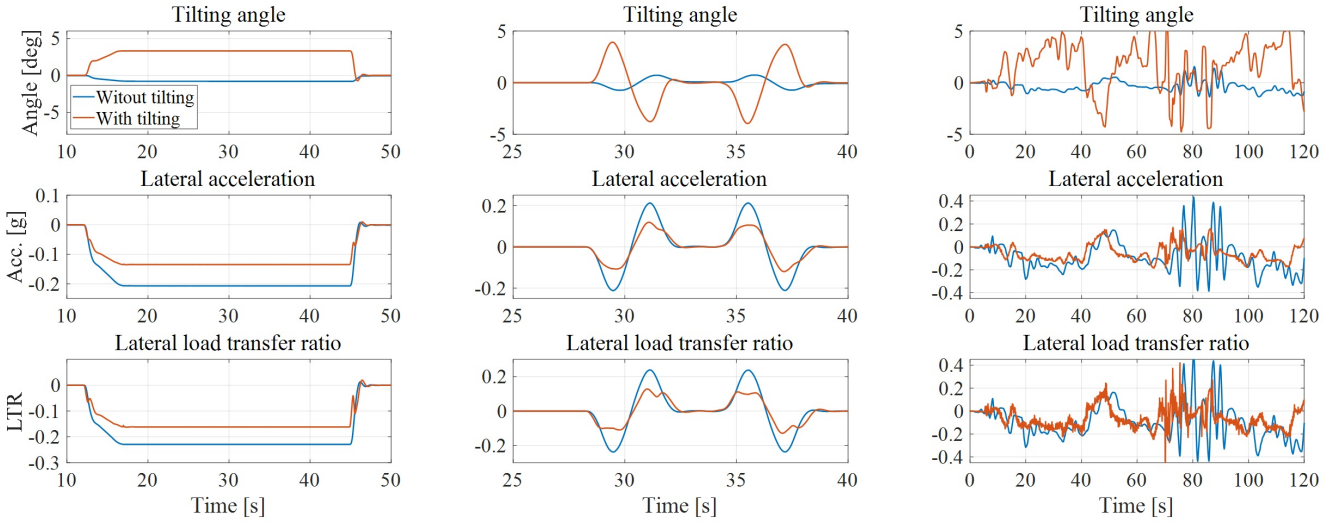

Fig. 10: HILS results comparing non-tilting and tilting: (a) constant radius cornering; (b) double lane change; (c) free driving

I/O interface linked to a hardware bench that includes a load actuator. The actuator reproduces the roll moments seen in driving so that the bench experiences realistic external forces. The measured tilting angle angle from the bench is fed back to CarSim, forcing the simulated mobility body to follow the hardware roll motion. This closed interaction enables repeatable evaluation while preserving actuator limits, gearbox friction, sensor noise, and computation delays observed in practice.

Two operating modes are supported. In the autonomous mode, speed and steering profiles are prescribed to enable objective performance assessment. In the manual (driver-in-the-loop) mode, a human driver operates the simulator to examine closed-loop feel and responsiveness in real time.

Three scenarios are used throughout this work:

- Constant-radius cornering: $v_x = 35$ km/h, $R = 30$ m.
- Double lane change: $v_x = 30$ km/h following ISO-style waypoints.
- Manual driving: driver-in-the-loop on a curved course.

Rollover safety is evaluated with two metrics. First, the driver-perceived lateral acceleration (from the tilting angle sensor frame aligned with the cabin) indicates comfort improvement due to tilting. Second, the LTR quantifies the vertical-load difference between left and right wheels:

$$\mathrm{LTR} \triangleq \frac{F_{z,l} - F_{z,r}}{F_{z,l} + F_{z,r}}, \tag{33}$$

where $F_{z,l}$ is the vertical force of the left wheel and $F_{z,r}$ is the vertical force of the right wheel. LTR values near 0 indicate stability and values approaching ± 1 indicate imminent wheel lift.

E. Results and discussion

Figure 10 summarizes the HILS results for the three scenarios, comparing a non-tilting baseline (motor shaft fixed) with the proposed tilting control. Across all cases, the mobility leans toward the inside of the turn, and both the perceived lateral acceleration and the magnitude of LTR decrease relative to the baseline, confirming improved rollover stability. The reduction is most visible in steady cornering, where the target generator aligns apparent gravity with the cabin vertical.

The DOB primarily reduces inner-loop tracking error by canceling low-frequency load disturbances and model error. Under the controlled conditions of the HILS tests, overall stability metrics with and without DOB are similar, but angle tracking accuracy improves with DOB. The benefit of DOB is expected to be more pronounced under real disturbances such as crosswinds, camber changes, or rough pavement.

V. CONCLUSIONS

This paper introduced and analyzed a suspension-integrated tilting mechanism for narrow-track mobility, wherein the MacPherson upper mounts connect to an actuated tilting plate. The resulting 2-DOF roll path was captured by a control-oriented, small-angle model derived via an energy formulation, providing state-space model and a torque-to-tilting angle transfer function. Building on this model, we implemented a dual-layer control structure: an tilt-reference generator that maps steering and speed to a target tilt for reducing perceived lateral acceleration, and an tilt-tracking controller that tracks the reference using feedback, feedforward, and a disturbance observer about a nominal second-order plant. HILS-based studies across constant-radius cornering, double lane change, and free driving scenarios exhibited consistent inside-leaning behavior and reductions in perceived lateral acceleration and LTR magnitude relative to a fixed-tilt baseline, while the disturbance observer improved tracking quality. In addition, the design addresses steering-tilting interaction by passively

generating a small counter-steer via bump-steer tuning to preserve curvature.

Current limitations arise from the small-angle treatment, simplified and linearlized modeling, and the use of nominal parameters in the tilt-tracking controller; these are partially mitigated by the disturbance observer and by HILS validation. Future work will incorporate tire compliance and sideslip dynamics into the plant, extend the tilt-reference generator toward predictive stability metrics (e.g., LTR-based preview or model predictive control), and conduct road tests to assess robustness against crosswinds, uneven surfaces, and broader driver inputs, as well as to refine the steering–tilting coordination.

REFERENCES

[1] K. M. Kockelman and Y. Zhao, "Behavioral Distinctions: The Use of Light-Duty Trucks and Passenger Cars," *Journal of Transportation and Statistics*, vol. 3, no. 3, pp. 47–60, 2000.

[2] W. A. Grzegożek, "Analysis of a Construction Solution for Narrow Track Vehicle (NTV)," *IOP Conference Series: Materials Science and Engineering*, vol. 421, no. 2, 022012, 2018.

[3] A. van Poelgeest, *The Dynamics and Control of a Three-Wheeled Tilting Vehicle*. Ph.D. thesis, University of Bath, 2011.

[4] M. Chatterjee, M. Kale, and B. N. Chaudhari, "Mathematical Modelling of Chassis Dynamics of Electric Narrow Tilting Three Wheeled Vehicle," in *Proc. IEEE INDICON*, 2015, pp. 1–6.

[5] J.-C. Chiou and C.-L. Chen, "Modeling and Verification of a Diamond-Shape Narrow-Tilting Vehicle," *IEEE/ASME Transactions on Mechatronics*, vol. 13, no. 6, pp. 678–691, 2008.

[6] J. J. H. Berote, J. Darling, and A. R. Plummer, "Development of a Tilt Control Method for a Narrow-Track Three-Wheeled Vehicle," *Proceedings of the Institution of Mechanical Engineers, Part D: Journal of Automobile Engineering*, vol. 226, no. 1, pp. 48–69, 2012.

[7] R. Rajamani, D. Piyabongkarn, V. Tsourapas, and J. Y. Lew, "Parameter and State Estimation in Vehicle Roll Dynamics," *IEEE Transactions on Intelligent Transportation Systems*, vol. 12, no. 4, pp. 1558–1567, 2011.

[8] C. Tang and A. Khajepour, *Narrow Tilting Vehicles: Mechanism, Dynamics, and Control*. San Rafael, CA, USA: Morgan & Claypool, 2019.

[9] D. Navikas and A. Pitrėnas, "Determination and Evaluation of a Three-Wheeled Tilting Vehicle Prototype's Dynamic Characteristics," *Applied Sciences*, vol. 12, no. 10, 5121, 2022.

[10] C. Tang, L. He, and A. Khajepour, "Design and Analysis of an Integrated Suspension Tilting Mechanism for Narrow Urban Vehicles," *Mechanism and Machine Theory*, vol. 120, pp. 225–238, 2018.

[11] R. Gao, H. Li, W. Wei, and Y. Wang, "Research on the Decoupling of the Parallel Vehicle Tilting and Steering Mechanism," *Applied Sciences*, vol. 12, no. 15, 7502, 2022.

[12] C. Larish, D. Piyabongkarn, V. Tsourapas, and R. Rajamani, "A New Predictive Lateral Load Transfer Ratio for Rollover Prevention Systems," *IEEE Transactions on Vehicular Technology*, vol. 62, no. 7, pp. 2928–2936, 2013.

[13] X. Ding, Z. Wang, and L. Zhang, "A Vehicle Rollover Prediction System Based on Lateral Load Transfer Ratio," in *Proc. Chinese Automation Congress (CAC)*, 2020, pp. 7256–7261.

[14] V. Tsourapas, D. Piyabongkarn, A. C. Williams, and R. Rajamani, "New Method of Identifying Real-Time Predictive Lateral Load Transfer Ratio for Rollover Prevention Systems," in *Proc. American Control Conference (ACC)*, 2009, pp. 439–444.

[15] S. Kidane, R. Rajamani, L. Alexander, P. J. Starr, and M. Donath, "Development and Experimental Evaluation of a Tilt Stability Control System for Narrow Commuter Vehicles," *IEEE Transactions on Control Systems Technology*, vol. 18, no. 6, pp. 1266–1279, 2010.

[16] R. Rajamani, J. Gohl, L. Alexander, and P. Starr, "Dynamics of Narrow Tilting Vehicles," *Mathematical and Computer Modelling of Dynamical Systems*, vol. 9, no. 2, pp. 209–231, 2003.

[17] D. Piyabongkarn, T. Keviczky, and R. Rajamani, "Active Direct Tilt Control for Stability Enhancement of a Narrow Commuter Vehicle," *International Journal of Automotive Technology*, vol. 5, no. 2, pp. 77–88, 2004.

[18] C. Tang, M. Ataei, and A. Khajepour, "A Reconfigurable Integrated Control for Narrow Tilting Vehicles," *IEEE Transactions on Vehicular Technology*, vol. 68, no. 1, pp. 234–244, 2019.

[19] C. Tang and A. Khajepour, "Integrated Stability Control for Narrow Tilting Vehicles: An Envelope Approach," *IEEE Transactions on Intelligent Transportation Systems*, vol. 22, no. 5, pp. 3158–3166, 2021.

[20] J. W. Robertson, *Active Control of Narrow Tilting Vehicle Dynamics*. Ph.D. thesis, University of Bath, 2014.

[21] C. Tang, *Narrow Urban Vehicles with an Integrated Suspension Tilting System: Design, Modeling, and Control*. M.A.Sc. thesis, University of Waterloo, 2018.

[22] Y. Ren, T. Q. Dinh, J. Marco, D. Greenwood, and C. Hessar, "Nonlinearity Compensation Based Tilting Controller for Electric Narrow Tilting Vehicles," in *Proc. IEEE Int. Conf. on Control, Decision and Information Technologies (CoDIT)*, 2018, pp. 1–6.